Into the depths: Techniques for in vitro three-dimensional microtissue visualization

Pranita K. Kabadi[1,*], Marguerite M. Vantangoli[1,*], April L. Rodd[1], Elizabeth Leary[2], Samantha J. Madnick[1], Jeffrey R. Morgan[2], Agnes Kane[1], and Kim Boekelheide[1]
[1]Department of Pathology and Laboratory Medicine and [2]Department of Molecular Pharmacology, Physiology and Biotechnology, Brown University, Providence, RI

*P.K.K. and M.M.V. contributed equally to this work

BioTechniques 59:279-286 (November 2015) doi 10.2144/000114353
Keywords: three-dimensional; microtissues; spheroids; clearing; histology

Supplementary material for this article is available at www.BioTechniques.com/article/114353.

Three-dimensional (3-D) in vitro platforms have been shown to closely recapitulate human physiology when compared with conventional two-dimensional (2-D) in vitro or in vivo animal model systems. This confers a substantial advantage in evaluating disease mechanisms, pharmaceutical drug discovery, and toxicity testing. Despite the benefits of 3-D cell culture, limitations in visualization and imaging of 3-D microtissues present significant challenges. Here we optimized histology and microscopy techniques to overcome the constraints of 3-D imaging. For morphological assessment of 3-D microtissues of several cell types, different time points, and different sizes, a two-step glycol methacrylate embedding protocol for evaluating 3-D microtissues produced using agarose hydrogels improved resolution of nuclear and cellular histopathology characteristic of cell death and proliferation. Additional immunohistochemistry, immunofluorescence, and in situ immunostaining techniques were successfully adapted to these microtissues and enhanced by optical clearing. Utilizing the Clear^{T2} protocol greatly increased fluorescence signal intensity, imaging depth, and clarity, allowing for more complete confocal fluorescence microscopy imaging of these 3-D microtissues compared with uncleared samples. The refined techniques presented here address the key challenges associated with 3-D imaging, providing new and alternative methods in evaluating disease pathogenesis, delineating toxicity pathways, and enhancing the versatility of 3-D in vitro testing systems in pharmacological and toxicological applications.

Current strategies for studying disease mechanisms, pharmaceutical drug discovery, and toxicity testing rely on in vivo animal and two-dimensional (2-D) in vitro models. Though commonly used to investigate disease pathogenesis and perform toxicity testing, animal models are not necessarily predictive of human responses following exposure, and interspecies differences can have profound impacts on extrapolation or interpretation of data (1). Animal models are limited by time intensive, costly, and low-throughput experiments, contributing to the large backlog of compounds that have not been adequately tested for safety (2–6). While in vitro–based models address these limitations, 2-D monolayer cultures lack the complex cell–cell interactions, intercellular junctions, cross-talk, and cellular morphology present in the in vivo environment (7,8).

Since standard in vitro culture systems and in vivo animal models are handicapped in their ability to recapitulate human tissue responses, there exists a need to develop more complex predictive systems to evaluate disease mechanisms and to serve as platforms for toxicological testing (7,9,10). In 2007, the NRC report "Toxicity Testing in the 21st Century: A Vision and a Strategy" (11) called for a change in the current approach to toxicity testing by emphasizing the development and use of more relevant in vitro systems using human cells.

New approaches for three-dimensional (3-D) cell culture have allowed increased cell–cell interactions, formation of intercellular junctions, and intercellular communication, providing a more physiologically relevant microsystem (8,10,12). Toxicity testing of compounds, including chemotherapeutics and nanoparticles, has demon-

METHOD SUMMARY

Here we present a summary of refined techniques for imaging of 3-D microtissues produced using agarose hydrogels. These techniques include adaptation of a two-step glycol methacrylate embedding protocol, immunostaining, and optical clearing, which improved the visualization of 3-D microtissues.

strated different responses in cells cultured in 2-D versus 3-D (10,13,14). However, the adaptation of 2-D fluorescence or imaging-based assays for use in 3-D models presents a serious challenge for 3-D in vitro cell culture. Imaging and visualization of structures is challenging in 3-D cell culture due to factors such as microtissue thickness, light scattering, and impaired diffusion of reagents across multiple cell layers (15).

Here we adapted and refined techniques that enable optimal visualization of microtissues to enhance imaging acquisition and assessment of morphological and toxicological outcomes relevant to human disease. To address the challenges associated with visualization, this study describes novel protocols for histopathology and optical clearing methods for imaging of 3-D microtissues produced using agarose hydrogels to obtain morphological and functional end points. Overall, the improved imaging and generation of integrated data sets will lead to expanded use of these 3-D microtissues for assessing toxicity.

Materials and methods

Culture methods

Culture methods and target cells are summarized in Table 1. BEAS-2B (No. CRL-9609; ATCC, Manassas, VA) immortalized human lung epithelial cells were cultured in BEGM media with a Single Quot supplement kit (No. CC-3170; Lonza, Basel, Switzerland) at 37°C in 5% CO_2. LNCaP (No. CRL-1740; ATCC) human prostate adenocarcinoma cells were cultured using phenol-red free RPMI-1640 (No. 11835; Life Technologies, Grand Island, NY) with 10% fetal bovine serum (FBS) and penicillin/streptomycin at 37°C in 5% CO_2. PLHC-1 (No. CRL-2406; ATCC) fish (*Poeciliopsis lucida*) hepatoma cells were cultured using EMEM media (No. 30–2003; ATCC) with 5% FBS and penicillin/streptomycin at 30°C in 5% CO_2.

3-D culture methods

Hydrogels containing 2% agarose were created from micromolds (No. 24–9; Microtissues, Inc., Providence, RI). Hydrogels were equilibrated with appropriate cell culture medium for a minimum of 30 min prior to cell seeding (16) into hydrogels at various densities (Table 1). After seeding, cells settled to the bottom of the small recesses and self-assembled into spheroids over the course of 24 h.

Microtissue histology

Microtissues within agarose hydrogels were fixed in 10% neutral buffered formalin (No. 225; Fisher Scientific, Agawam, MA) for a minimum of 24 h prior to dehydration and processing. Microtissues within the agarose molds were then embedded in Technovit 7100 glycol methacrylate (No. 14653I; Electron Microscopy Sciences, Hatfield, PA) per manufacturer's specifications with one modification. Samples were partially submerged in the infiltration solution and hardener 2 mixture to allow the sample to firmly attach to the bottom of the histology mold prior to filling the mold completely and adding a block holder. Samples were sectioned at a thickness of 3 μm, after which sections were mounted on slides and stained with hematoxylin and eosin (H&E) for histological examination.

Preparation of frozen sections

Microtissues within agarose hydrogels were fixed in 10% neutral buffered formalin overnight at 4°C. Following fixation and 2 washes with phosphate-buffered saline (PBS), samples were placed in a 15% sucrose/PBS solution for at least 3 h at room temperature and then in a 30% sucrose/PBS solution overnight at 4°C. Samples were embedded in optimal cutting temperature compound (OCT) (No. 14–373–65, Tissue–Tek; Fisher Scientific), frozen on dry ice before sectioning, and stored at -80°C until use. Samples were sectioned at 8 μm and affixed to Superfrost plus slides (No. 12–55–010; Fisher Scientific) before storage at -80°C until immunostaining.

Immunohistochemistry

Frozen sections of microtissues affixed to slides were thawed, dried at room temperature, and washed in PBS twice prior to antigen retrieval. For antigen retrieval, samples were placed in pre-heated 0.01 M citrate buffer (pH 6.0) for 20 min and then allowed to cool for 20 min. After 2 washes in PBS (5 min each), slides were treated with a 3% peroxide/methanol solution to quench endogenous peroxidase activity. Sections were then incubated with an Avidin/Biotin Block Kit (No. SP-2100; Vector Laboratories, Burlingame, CA) per manufacturer's specifications and blocked in a 1% bovine serum albumin (BSA) (No. A7906; Sigma-Aldrich, St. Louis, MO) and 15% goat serum (No. G9023; Sigma-Aldrich) solution for 1 h at room temperature. Slides were incubated overnight with an anti-E-cadherin primary antibody (1:6000 dilution) (No. 610181; BD Biosciences, San Jose, CA) at 4°C. Following washes in PBS, samples were incubated with goat anti-mouse IgG biotinylated secondary antibody (1:1000 dilution) (No. B0529; Sigma-Aldrich) for 1 h at room temperature and subsequent incubation with Avidin/Biotin Peroxidase Complex Kit (PK-6100; Vector Laboratories) per manufacturer's recommendation. Antibody expression was detected using the DAB Kit (No. SK-4100; Vector Laboratories). Sections were then counterstained with hematoxylin and coverslipped with Cytoseal 60 (No. 23–244257; Thermo Fisher Scientific, Waltham, MA).

Immunofluorescence of frozen sections

Frozen sections affixed to slides were allowed to warm to room temperature and then fixed for 5 min in 4% paraformaldehyde or 10% neutral buffered formalin. Slides were washed with PBS 3 times at room temperature and then permeabilized with 0.25% Triton X-100 for 10 min at room temperature. Samples were washed in PBS as before and then blocked with 1% goat serum, 3% BSA, and 0.3 M glycine for 1 h at room temperature. Slides were incubated overnight at 4°C with same anti-E-cadherin antibody (1:500 dilution) used for immunohistochemistry as described above. Following incubation, slides were washed in PBS as described above and incubated with anti-mouse secondary antibody (1:1000 dilution) (No.

Table 1. Cell culture conditions.

Cell line	Cell type	Media and supplements	Temperature	Microtissues, Inc. Mold	Seeding density/gel	Cells/ microtissue
BEAS-2B	Human lung epithelium	BEGM media with Single Quot supplement kit	37°C	24–35	80,000	2300
				24–96	80,000	830
LNCaP	Human prostate adenocarcinoma	RPMI 1640 with 10% FBS and penicillin/streptomycin	37°C	12–256	95,000	375
PLHC-1	*Poeciliopsis lucida* hepatocyte	EMEM with 5% FCS and penicillin/streptomycin	30°C	24–96	100,000	1050

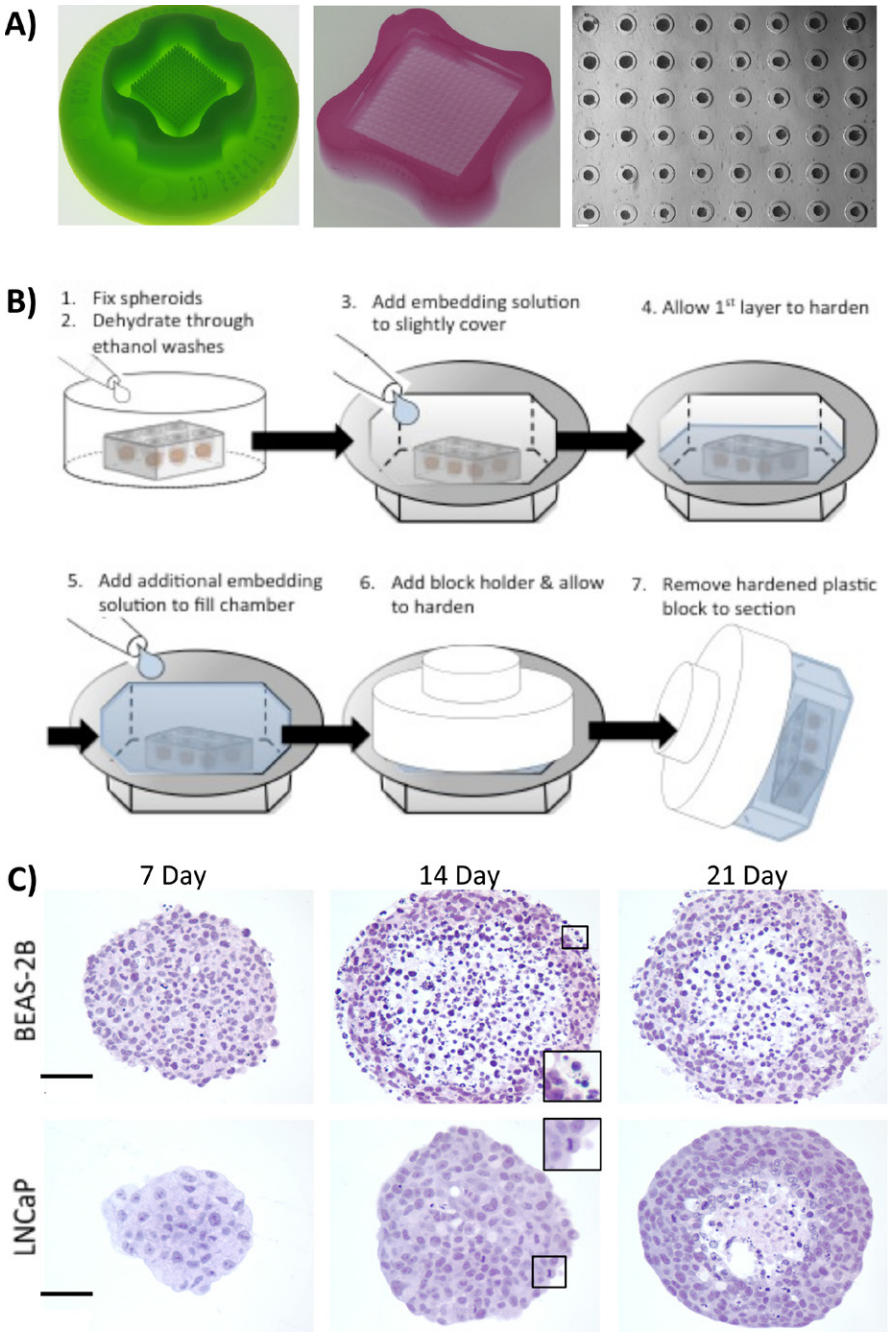

Figure 1. 3-D microtissue embedding and histopathology. (A) Micromolds were used to cast agarose hydrogels containing 256 round-bottom recesses for microtissue formation. (B) An array of microtissues can be processed for imaging directly in the hydrogels, as shown in the diagram of the two-step plastic embedding and histology process. (C) H&E staining of BEAS-2B (top panel) and LNCaP (bottom panel) microtissues show normal morphology at 7 days and proliferating and apoptotic cells after 14 days (see figure insets). Scale bar = 50 µm.

A21236; Life Technologies) for 2 h at room temperature. For F-actin staining to visualize the cytoskeleton, sections were permeabilized as above and incubated with rhodamine phalloidin (1:500 dilution) (R415; Life Technologies) for 25 min. Slides were washed as described above and stained with Hoechst 33342 (1:1000 dilution) (No. H1399; Life Technologies) for 30 min at room temperature. Coverslips were mounted using hard set mounting media (No. H-1400; Vector Laboratories) and stored in the dark at 4°C until imaging.

Immunofluorescence of whole spheroids

Whole microtissues in agarose hydrogels were fixed in 10% neutral buffered formalin overnight at 4°C. Following fixation, gels were washed with PBS 3 times for 5 min each at room temperature with gentle shaking. Spheroids were permeabilized by incubation in 0.25% Triton X-100 in PBS for 2 h at room temperature and washed as described above. Samples were blocked for 1 h at room temperature with 1% goat serum, 3% BSA, and 0.3 M glycine, followed by incubation with the same anti-E-cadherin antibody (1:500 dilution) mentioned above overnight at 4°C. Samples were then washed in PBS as previously described and incubated with anti-mouse secondary antibody (1:1000 dilution) for 2 h at room temperature followed by washes as described above, counterstained with Hoechst 33342 (1:2000 dilution) for 2 h at room temperature followed by additional PBS washes, and finally, protected from light during storage at 4°C until clearing. For Hoechst staining alone, previously fixed microtissues stored at 4°C were stained with Hoechst 33342 (1:2000 dilution) in PBS for 2 h at room temperature.

Detection of reactive oxygen species (ROS)

BEAS-2B microtissues were grown for 4 days, then treated with 50 µM menadione sodium bisulfite (No. M5750; Sigma-Aldrich) and counterstained with Hoechst 33342 (1:2000 dilution) for 1 h. After 1 h, 5 µM CellROX Green reagent (No. C1044; Life Technologies) was added to each sample for an additional hour as per manufacturer's suggestions. Samples were briefly washed in PBS twice for 5 min and fixed in 10% neutral buffered formalin for 1 h before being cleared and imaged using a Zeiss LSM710 laser confocal microscope (Carl Zeiss, Jena, Germany).

Clear^{T2} optical clearing

Samples were cleared in a chemical fume hood using a modified version of the original Clear^{T2} protocol developed by Kuwajima et al. (2013). The methods were adapted to microtissues and required a 1 h incubation of samples in a final solution of 50% formamide (No. 47670; Sigma-Aldrich) and 20% polyethylene glycol (PEG) (No. 89510I Sigma-Aldrich). For imaging of intact microtissues, agarose hydrogels were inverted and placed into 35 mm glass bottom dishes (No. P35G; MatTek, Ashland, MA) to allow samples to fall out of hydrogels and onto the coverslips for imaging using laser scanning confocal microscopy and a 20× objective (Zeiss LSM710, Plan-Apochromat, 0.8 NA, 0.55 WD objective). During imaging, plates were sealed with parafilm to prevent evaporation of formamide.

Results and discussion

The adaptation of 2-D imaging-based assays to 3-D culture models has presented significant issues, including problems with clear visualization and penetration of reagents into the cores of 3-D microtissues. Addressing these challenges required the development of new approaches to evaluate relevant toxicological and morphological end points by merging standard in vivo histological techniques with faster in vitro assays, bridging the gap between in vivo and in vitro toxicological and pharmacological studies.

Improved histological techniques for imaging of 3-D microtissues

Self-assembly of 3-D microtissues created using non-adhesive agarose hydrogels (16) (Figure 1A) occurred over the course of the first 20 h after seeding. The process can be optimized to control spheroid size by regulating seeding density to yield a specific diameter after a given time point (Figure 1C). Traditional histological techniques were adapted to enable visualization of microtissue interiors. A two-step amendment to the Technovit 7100 plastic histology protocol enabled en-bloc embedding with minimal disruption to whole hydrogels containing an array of 256 microtissues per section (Figure 1, A and B). H&E staining of 3 μm BEAS-2B (Figure 1C, top panel) and LNCaP microtissue sections (Figure 1C, bottom panel) permitted close examination of nuclear, cellular, and overall tissue morphology. These key changes in cellular structure were easily distinguishable within the histological samples, emphasizing the advantage provided by the clarity of the thin plastic sections for identifying key cellular and morphological features (Figure 1C).

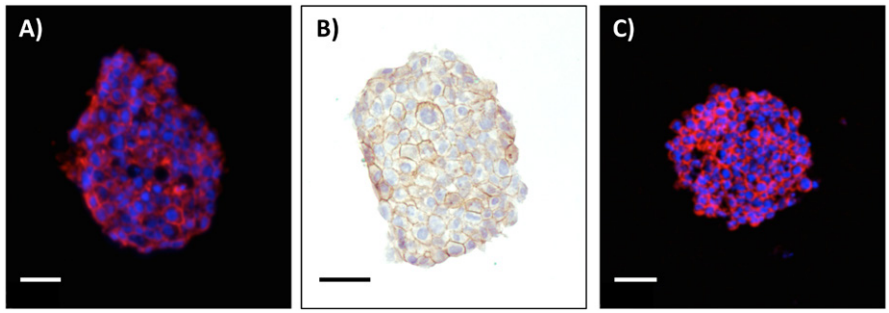

Figure 2. Immunostaining of frozen 3-D microtissue sections at 3 days. E-cadherin was localized in LNCaP microtissues by (A) immunofluorescence using an anti-E-cadherin antibody (red) and Hoechst 33342 nuclear counterstain (blue) or (B) immunohistochemistry with an anti-E-cadherin antibody (dark brown) and hematoxylin nuclear counterstain (blue). (C) BEAS-2B cells visualized using fluorescence [nuclear staining (blue) and F-actin staining with rhodamine phalloidin (red)]. Scale bar = 50 μm.

Histopathological assessment of tissue-like interactions is important in assessing adverse end points as complex cellular interactions and tissue organization are lacking in traditional 2-D in vitro cultures. Histology of microtissues at 7 and 14 days exhibited mitotic figures and long-term cell viability was indicated by intact nuclear and cytoplasmic structures at 21 days in culture (inset image, Figure 1C). Although microtissues were viable after 21 days, both BEAS-2B and LNCaP cultures at 14 and 21 days contained areas of cell death and cellular debris at the core (inset image, Figure 1C). The observed cell

death is most likely due to increased microtissue diameter, as previous studies have reported a 100 μm diffusion limit of oxygen and other nutrients within various 3-D cell culture models (17,18). Exploiting these limitations may be advantageous in mimicking hypoxic tumor environments to model tumor progression and response to cancer therapies (19–21). These techniques may be applicable to other hydrogel and scaffold-free models; however, 3-D cultures require more arduous collection and embedding protocols for histology, as seen with PLHC-1 microtissues (Supplementary Figure S1). The ability to manipulate microtissue size, visualize microtissue cores, and assess morphologies using these refined histological techniques accentuates the strength of 3-D in vitro models as alternative methods for addressing a wide variety of pharmaceutical and toxicity testing needs.

Immunostaining of 3-D microtissues

To demonstrate the versatility of 3-D microtissues, new approaches for histological and immunostaining techniques were examined. Fixed agarose hydrogels containing microtissues were en-bloc embedded in OCT with a two-step embedding protocol similar to the glycol methacrylate embedding procedure. Immunofluorescence and immunohistochemistry of LNCaP microtissue sections showed strong staining for the epithelial cell marker E-cadherin at cell–cell junctions (Figure 2, A and B). This technique was also validated using rhodamine phalloidin to visualize cellular F-actin staining and cytoskeletal organization in BEAS-2B microtissue sections (Figure 2C). Similar to tissue arrays, fixing, embedding and sectioning the whole agarose hydrogel also enables uniform staining, visualization, and assessment of multiple microtissues within a single sample (22–24). Additional samples fixed in Optimal Fix (American MasterTech Scientific, Inc., Lodi, CA), an alcohol-based fixative, were similarly embedded but yielded poor results during cryosectioning due to a lack of proper OCT infiltration in the hydrogel (data not shown). The current study demonstrates the utility and practicality of protein biomarker assessment using immunostaining of 3-D cultures to visualize specific structures and patterns of expression within microtissues.

Clearing for improved optical imaging of 3-D microtissues

Imaging of intact 3-D samples was greatly improved through the use of optical clearing protocols, allowing for faster and higher-throughput fluorescence imaging of spheroids in situ. In this study, an organic solvent-free method for optical clearing, Clear^{T2}, improved imaging depth and greatly increased the number of discernible fluorescently labeled nuclei in PLHC-1 microtissues compared with uncleared samples imaged in PBS (Figure 3A). The Clear^{T2} protocol enabled sharper visualization of nuclear structure, particularly in the center of the microtissue at a depth of more than 75 μm along the z-axis, in stark contrast to nuclear staining of uncleared samples, which was obscured or indistinct at depths greater than 30 μm (Figure 3A, Supplementary Videos 1A and 1B).

The Clear^{T2} method was also used in conjunction with immunostaining and biochemical staining of microtissues, demonstrating the advantages of this technique in evaluating important functional and toxicity end points. LNCaP microtissues, which were stained and cleared in situ, showed localization of E-cadherin staining at cell–cell contacts (red) and clearly visible nuclear staining (gray) throughout each sequential image in the z-axis (Figure 3B, Supplementary Videos 2A and 2B). In addition to evaluating the formation of cell–cell junctions as a functional end point, toxicological end points such as oxidant generation can also be examined in intact spheroids. To induce the generation of reactive oxygen species (ROS), BEAS-2B microtissues were treated with menadione sodium bisulfite, a redox-cycling compound, prior to staining with CellROX green to detect ROS generation and nuclear counterstaining (gray, Figure 3B). Cleared samples (Figure 3B, bottom panel) showed increased optical imaging of the microtissue interior with more distinct cellular staining compared with uncleared samples in PBS (Figure 3B, top panel), indicating that dye penetration into the microtissue was not a limiting factor. However, optimization

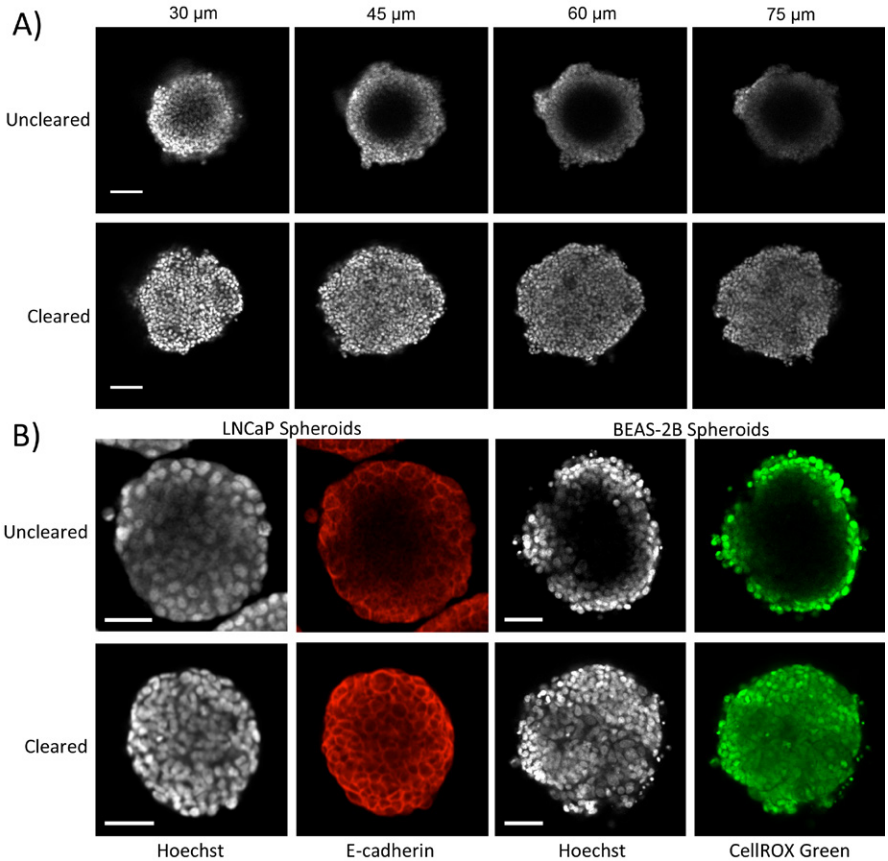

Figure 3. Confocal fluorescence imaging of spheroids is improved by clearing. (A) PLHC-1 spheroids were imaged in PBS without clearing (top panel) or with clearing by formamide and polyethylene glycol (PEG) (bottom panel), after nuclear staining (gray). Confocal cross-section images (left-to-right) were taken every 15 μm along the z-axis. (B) Confocal cross-sections (z-axis) through the middle of LNCaP spheroids (stained for E-cadherin) and BEAS-2B spheroids (induced with 50 μM menadione and stained with CellROX Green) imaged 3 days after staining. Both microtissues were counterstained for nuclei (gray), and visualized in PBS without clearing (top panel) or after clearing with formamide and PEG prior to imaging (bottom panel). Scale bar = 50 μm.

of immunostaining protocols was critical in alleviating the challenges of imaging in 3-D. The use of un-optimized protocols did not produce adequate immunostaining in microtissues despite the applied clearing method, emphasizing the necessity of refining techniques specifically for 3-D in vitro assays (Supplementary Figure S2, Supplementary Videos 3A and 3B). The staining and clearing of intact microtissues can be applied to other scaffold-free models as demonstrated in Supplemental Figure S3. Our adaptation of the Clear^{T2} method successfully cleared human and fish microtissues in less than 2 h, validating the efficiency and efficacy of this technique in multiple species and establishing the potential of 3-D in vitro testing platforms in fields such as environmental and aquatic toxicology.

These results from the first application of the Clear^{T2} method for increased visualization of fluorescence in non-neuronal microtissues demonstrate enhanced resolution and imaging depth when visualizing intact 3-D microtissues. A variety of clearing solutions, including the solvent-based methods 3-DISCO (3-D imaging of solvent cleared organs) and BABB (utilizing a 1:2 mix of benzyl alcohol and benzyl benzoate), have previously been developed for the visualization of thick tissues and have been applied to a wide range of samples derived from brain, skin, mammary glands, immune organs, whole embryos, and other tissues from in vivo and in vitro experiments (20,25–30). In contrast to other protocols, Clear^{T2} is fast, detergent-free, and immersion-based, which are ideal characteristics for 3-D in vitro applications and toxicity testing (15,25–28,31). A recent study compared multiple clearing methods using neuronal microtissues and determined that Clear^{T2} increased the fluorescence signal throughout the microtissue without altering tissue size, unlike other clearing protocols such as SeeDb and Scale. Improved resolution and increased imaging depth provide more complete imaging data sets, allowing for better quantification of morphological and phenotypic outcomes, with the potential to better understand heterogeneous cellular responses within a microtissue.

The use of non-adhesive micromold hydrogels to create 3-D multicellular in vitro microtissues provides an improved platform with the capability to merge the complexities of in vivo tissues with the advantages and practicality of 2-D in vitro models. The ability to clearly assess detailed morphology, evaluate longer-term end points using sub-lethal markers, and discern adaptive responses from acute toxicity is a major advantage of this 3-D model. The improved techniques presented in this study address the challenges of visualizing 3-D microtissues, highlighting their utility for evaluating classical pathological changes and laying the foundation for alterative platforms as efficient and effective screening tools with the potential to contribute to the ongoing revolution in toxicity testing (32).

The flexibility of the 3-D in vitro cell culture hydrogel microtissue platform is a major advantage, allowing the use of various cell types with improved delineation of biological pathways and mechanisms implicated in toxicity responses and disease pathogenesis. The improved histological and visualization techniques described in this study enhance the application, validity, and feasibility of 3-D in vitro model systems. These models and imaging methods have the potential for adaptation to high-throughput screening of primary or immortalized cells, thereby increasing the human relevance, efficiency, and efficacy of 3-D microtissue models for evaluating disease mechanisms, pharmaceutical drug discovery and toxicity testing.

Author contributions

P.K.K., M.M.V., A.L.R., E.L., and S.J.M. designed and conducted the experiments. P.K.K., M.M.V., A.L.R., and E.L. wrote the manuscript. J.R.M., A.K., and K.B. supervised the project. All authors contributed to revision of the manuscript.

Acknowledgements

This research is supported by NIEHS Training Grant T32 ES007272, the NIEHS Superfund Research Program P42 ES013660, BP/The Gulf of Mexico Research Initiative through the Consortium for Molecular Engineering of Dispersant Systems (CMEDS), and the generous gift of Donna McGraw Weiss '89 and Jason Weiss. This paper is subject to the NIH Public Access Policy.

Competing interests

J.R.M. has an equity interest Microtissues, Inc. K.B. is an occasional expert consultant for chemical and pharmaceutical companies and owns stock in Semma Therapeutics, a biotechnology company developing a cell-based therapy for diabetes.

References

1. **Knight, A.** 2007. Animal experiments scrutinised: systematic reviews demonstrate poor human clinical and toxicological utility. ALTEX *24*:320-325.
2. **Ennever, F.K. and L.B. Lave.** 2003. Implications of the lack of accuracy of the lifetime rodent bioassay for predicting human carcinogenicity. Regul Toxicol Pharmacol. *38*:52-57.
3. **Olson, H., G. Betton, D. Robinson, K. Thomas, A. Monro, G. Kolaja, P. Lilly, J. Sanders, et al.** 2000. Concordance of the toxicity of pharmaceuticals in humans and in animals. Regul Toxicol Pharmacol. *32*:56-67.
4. **Shanks, N., R. Greek, and J. Greek.** 2009. Are animal models predictive for humans? Philos. Ethics Humanit. Med. *4*:2.
5. **Johnson, D.E. and G.H. Wolfgang.** 2000. Predicting human safety: screening and computational approaches. Drug Discov. Today *5*:445-454.
6. **Sun, H., M. Xia, C.P. Austin, and R. Huang.** 2012. Paradigm shift in toxicity testing and modeling. AAPS J. *14*:473-480.
7. **Maltman, D.J. and S.A. Przyborski.** 2010. Developments in three-dimensional cell culture technology aimed at improving the accuracy of in vitro analyses. Biochem. Soc. Trans. *38*:1072-1075.
8. **Wang, W., K. Itaka, S. Ohba, N. Nishiyama, U.I. Chung, Y. Yamasaki, and K. Kataoka.** 2009. 3-D spheroid culture system on micropatterned substrates for improved differentiation efficiency of multipotent mesenchymal stem cells. Biomaterials *30*:2705-2715.
9. **Astashkina, A.I., B.K. Mann, G.D. Prestwich, and D.W. Grainger.** 2012. Comparing predictive drug nephrotoxicity biomarkers in kidney 3-D primary organoid culture and immortalized cell lines. Biomaterials *33*:4712-4721.
10. **Lee, J., G.D. Lilly, R.C. Doty, P. Podsiadlo, and N.A. Kotov.** 2009. In vitro toxicity testing of nanoparticles in 3-D cell culture. Small *5*:1213-1221.
11. **Krewski, D., D. Acosta, Jr., M. Andersen, H. Anderson, J.C. Bailar 3rd, K. Boekelheide, R. Brent, G. Charnley, et al.** 2010. Toxicity testing in the 21st century: a vision and a strategy. J. Toxicol. Environ. Health B Crit. Rev. *13*:51-138.
12. **Bhadriraju, K. and C.S. Chen.** 2002. Engineering cellular microenvironments to improve cell-based drug testing. Drug Discov. Today *7*:612-620.
13. **Pickl, M. and C.H. Ries.** 2009. Comparison of 3-D and 2-D tumor models reveals enhanced HER2 activation in 3-D associated with an increased response to trastuzumab. Oncogene *28*:461-468.
14. **Sun, T., S. Jackson, J.W. Haycock, and S. MacNeil.** 2006. Culture of skin cells in 3-D rather than 2-D improves their ability to survive exposure to cytotoxic agents. J. Biotechnol. *122*:372-381.
15. **Boutin, M.E. and D. Hoffman-Kim.** 2015. Application and assessment of optical clearing methods for imaging of tissue-engineered neural stem cell spheres. Tissue Eng. Part C Methods *21*:292-302.
16. **Napolitano, A.P., D.M. Dean, A.J. Man, J. Youssef, D.N. Ho, A.P. Rago, M.P. Lech, and J.R. Morgan.** 2007. Scaffold-free three-dimensional cell culture utilizing micromolded nonadhesive hydrogels. Biotechniques *43*:494-500.
17. **Glicklis, R., J.C. Merchuk, and S. Cohen.** 2004. Modeling mass transfer in hepatocyte spheroids via cell viability, spheroid size, and hepatocellular functions. Biotechnol. Bioeng. *86*:672-680.
18. **Ong, S.M., Z. Zhao, T. Arooz, D. Zhao, S. Zhang, T. Du, M. Wasser, D. van Noort, and H. Yu.** 2010. Engineering a scaffold-free 3-D tumor model for in vitro drug penetration studies. Biomaterials *31*:1180-1190.
19. **Yamada, K.M. and E. Cukierman.** 2007. Modeling tissue morphogenesis and cancer in 3-D. Cell *130*:601-610.
20. **Hirt, C., A. Papadimitropoulos, V. Mele, M.G. Muraro, C. Mengus, G. Iezzi, L. Terracciano, I. Martin, and G.C. Spagnoli.** 2014. "In vitro" 3-D models of tumor-immune system interaction. Adv. Drug Deliv. Rev. *79-80*:145-154.
21. **Malda, J., T.J. Klein, and Z. Upton.** 2007. The roles of hypoxia in the in vitro engineering of tissues. Tissue Eng. *13*:2153-2162.
22. **Kayser, G., A. Csanadi, C. Otto, T. Plones, N. Bittermann, J. Rawluk, B. Passlick, and M. Werner.** 2013. Simultaneous multi-antibody staining in non-small cell lung cancer strengthens diagnostic accuracy especially in small tissue samples. PLoS ONE *8*:e56333.
23. **Camp, R.L., V. Neumeister, and D.L. Rimm.** 2008. A decade of tissue microarrays: progress in the discovery and validation of cancer biomarkers. J Clin Oncol. *26*:5630-5637.
24. **Bubendorf, L., A. Nocito, H. Moch, and G. Sauter.** 2001. Tissue microarray (TMA) technology: miniaturized pathology archives for high-throughput in situ studies. J. Pathol. *195*:72-79.
25. **Chung, K., J. Wallace, S.Y. Kim, S. Kalyanasundaram, A.S. Andalman, T.J. Davidson, J.J. Mirzabekov, K.A. Zalocusky, et al.** 2013. Structural and molecular interrogation of intact biological systems. Nature *497*:332-337.
26. **Ertürk, A. and F. Bradke.** 2013. High-resolution imaging of entire organs by 3-dimensional imaging of solvent cleared organs (3-Dros. Inf. Serv.CO). Exp. Neurol. *242*:57-64.
27. **Ertürk, A., K. Becker, N. Jahrling, C.P. Mauch, C.D. Hojer, J.G. Egen, F. Hellal, F. Bradke, et al.** 2012. Three-dimensional imaging of solvent-cleared organs using 3-Dros. Inf. Serv.CO. Nat. Protoc. *7*:1983-1995.
28. **Hama, H., H. Kurokawa, H. Kawano, R. Ando, T. Shimogori, H. Noda, K. Fukami, A. Sakaue-Sawano, and A. Miyawaki.** 2011. Scale: a chemical approach for fluorescence imaging and reconstruction of transparent mouse brain. Nat. Neurosci. *14*:1481-1488.
29. **Calle, E.A., S. Vesuna, S. Dimitrievska, K. Zhou, A. Huang, L. Zhao, L.E. Niklason, and M.J. Levene.** 2014. The use of optical clearing and multiphoton microscopy for investigation of three-dimensional tissue-engineered constructs. Tissue Eng. Part C Methods *20*:570-577.
30. **Zhu, D., K.V. Larin, Q. Luo, and V.V. Tuchin.** 2013. Recent progress in tissue optical clearing. Laser Photon Rev. *7*:732-757.
31. **Richardson, D.S. and J.W. Lichtman.** 2015. Clarifying Tissue Clearing. Cell *162*:246-257.
32. **Thoma, C.R., S. Stroebel, N. Rosch, B. Calpe, W. Krek, and J.M. Kelm.** 2013. A high-throughput-compatible 3-D microtissue co-culture system for phenotypic RNAi screening applications. J. Biomol. Screen. *18*:1330-1337.

Received 31 March 2015; accepted 31 August 2015.

Address correspondence to Kim Boekelheide, Department of Pathology and Laboratory Medicine, Brown University, Box G-E5, Providence, RI. E-mail: Kim_Boekelheide@brown.edu